UAV Group Design Project

Assignment 1

AER301

170153706 William Streuli

170154471 Chi Chung Kelvin Man

170154493 Thomas Parks

170154600 Ivan Ricote Sanchez

170154895 William Stokes-Roberts

190182641 Yanmin Guan

University of Sheffield

December 2019

Declaration Page

The University Of Sheffield.

Aerospace Engineering.

AER301/6001: Aerospace Group Design

Group:

		Student 1	Student 2	Student 3	Student 4	Student 5	Student 6	Student 7
Surname		Ricote Sanchez	Parkes	Streuli	Man	Guan	Stokes-Roberts	
Forename		Ivan	Thomas	William	Chi Chung Kelvin	Yanmin	William	
Reg. No.		170154600	170154493	170153706	170154471	190182641	170154895	
Signature								
Technical Area	a	50	80	45	100	0	0	
	b	0	20	5	0	0	50	
	c	50	0	45	0	100	0	
	d	0	0	5	0	0	50	

Note that each Technical Area is outlined in the Handbook in Section 2.1. A percentage should be allocated to each student for each of the applicable Technical Areas.

No total for any one student should exceed 100%, but a Technical Area can exceed 100% or be less.

By signing this sheet you acknowledge your satisfaction with all group member percentages of allocation

Contents

1 Introduction

In recent years the demand for Unmanned Aerial Vehicles (UAVs) has skyrocketed. Whether for military or for consumer use, they have developed into a broad range of aircraft varying from multi-rotors to fixed wing aircraft. These different types of UAVs vary in application; multi-rotors have taken the film industry by storm as their ability to carry heavy high-performing cameras means that directors can choose a much cheaper and much more manoeuvrable aerial photography source, as opposed to hiring manned helicopters. Unmanned fixed

wing aircraft have been widely introduced and accepted into multiple militaries across the globe. The unmanned aspect of the aircraft has multiple benefits. For example, the aircraft can be set to perform autonomous missions that last far longer than a human pilot onboard would be able to perform. This helps to prevent danger to the pilot as they can fly the UAV from a secure location. In addition, UAVs can provide greater levels of civilian safety due to the increased reconnaissance ability.

In this report, the entire engineering process behind creating a hobby grade fixed-wing UAV will be explained in detail. This UAV must be capable of performing a set mission autonomously whilst meeting set design criteria requirements. The project will test all the core attributes required of an engineer as the project must be well planned, be within its budget and meet deadlines for project milestones. To facilitate good time management, a Gantt chart for the Autumn semester was produced (Figure 1). This will help ensure that target deadlines are met and the project is efficiently completed. This will test problem-solving and team-working skills whilst under time and budget pressures and hence will be a realistic engineering project.

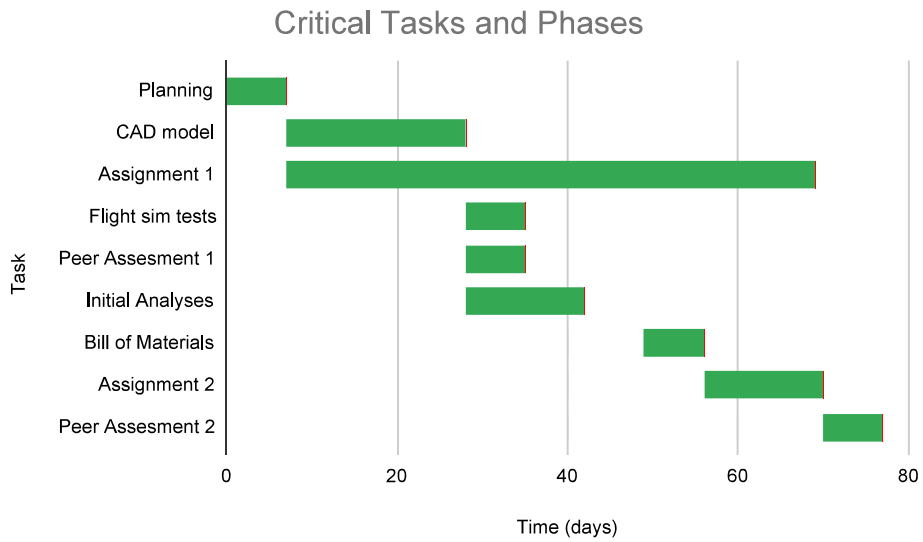

Figure 1: Autumn semester Gantt chart

Each design stage for the UAV will be explained and the subsequent design choices will be justified with numerical data and plots. These design justifi-

cations will show how decisions made will attain the best possible design that meets all requirements of the design criteria.

1.1 Conceptual Design

Before work could commence on the design of a UAV, a conceptual design phase took place in order to determine the requirements for the UAV. Ideas were proposed and each team member voted in so that the best design could be decided. In order to do this, the specification was first considered so that any design put forward would meet the criteria.

In the ideas proposed, number of motors used in the UAV was decided. Arguments of using one or two motors was raised, using one motor benefits the limited weight in the requirements, whereas using two motors would increase the power ratio compared to using one motor and aircraft can still be flyable from failure of one motor. Additionally, use of two motors allows yaw control by differential thrust in the event the rudder fails. Overall, a decision of 2 motors were made from team voting and would be put on the mid-wing of UAV. Effect on mid-wing increases the stability of the overall UAV as the weight would be closer to the centre of mass.

Wing position and type of wing was decided to be a diverged high wing and swept back wing type. With the limited width of 1 m, having a diverged wing design increases the available wing length, in which increases the overall lift of the UAV. High wings generally have an increase in the ground view and decreases the general effect wings have on the ground effect while landing. Swept wings is a wing angled backwards (or forwards) to a certain degree instead of having a straight sideways wing. Having a swept wing on the UAV makes the overall aerial vehicle more aerodynamic as this reduces drag. Finally, a H-shape tail helps reduce the effect of turbulent airflow and increases the lift at take-off since the overall area has increased.

A pull powertrain system was considered in the UAV, in conjunction with retractable landing gear, the drag is decreased leading to an improved climbing

performance and a higher cruise speed. Position of motors is also an important issue. High wing designs are commonly used within cargo aircraft due to the increased amount of space it affords as well as the reduction in ground effects. A low wing aircraft was ruled out due to the lack of space for wing-mounted engines. Mid wing aircraft have better rolling movements as well as rolling stability, however, a mid wing also comes with increased construction difficulties. After some discussion and debating, a mid-high wing design was chosen. The tail is designed to provide both stability and control of the aircraft. Most tail designs are split into two components. The horizontal tailplane contains the elevator while simultaneously providing counter-lift to stabilise the plane. The vertical tailplane contains the rudder and provides yaw stabilisation.

2 Materials and Structure

To continue the design process, the basic structure had to be defined and the material choices for each component. This allowed a CAD model to be constructed and computational analyses begun. These are essential to ensure the design will maximise its performance.

2.1 Material Selection

When choosing materials for various parts of the design, many factors must be taken into consideration. For the best performance, the lightest model is desirable. However, a balance must be struck between weight and strength to ensure the aircraft can endure the flight loads. Additionally, stiffness must be considered to avoid aeroelastic effects such as flutter, which could cause catastrophic failure in the correct circumstances.

For the spars, pultruded carbon fibre box or round section will be used, sourced from [1]. These sections are constructed from standard modulus fibres, with an epoxy resin matrix. Pultrusion is a high quality manufacturing process, allowing for high fibre volume fractions, while almost eliminating voids.

The fibres are laid unidirectionally for excellent bending resistance, however torsional stiffness may suffer. This can be mitigated by the use of two spars along the chord line, allowing the second moment of area to be greatly reduced, increasing rigidity.

Plywood will be used for the ribs due it's high strength and ease to manufacture with. The ribs will be cut in using a laser, allowing for precise cuts to ensure the two wings will be symmetrical. This will ensure that the aircraft will be stable and controllable in the air. Plywood is manufactured from multiple plies of wood veneer, with each layer being rotated to change the grain direction. This gives much more isotropic properties and prevents splitting along the grain. This is important for ribs as they are subject to widely varying forces and may bear a large impact in crashes, for example.

Plywood was chosen over a more traditional material such as balsa wood as it has better physical properties, namely fracture toughness. The primary physical properties of each are displayed in Table 1. Properties are taken in the longitudinal direction to give the most favourable properties. For balsa wood, properties in the transverse direction are poor. This is evident by its isotropy ratio of 10-30 [2]. Plywood shows much more similar values in directions both parallel and perpendicular to the face grain. Inter-laminar (out of plane) properties are much less important as loading conditions will not be high in this direction.

Physical Property	Wood Type	
	Balsa	Birch Ply
Density [kgm^{-3}]	280	686
Young's Modulus [GPa]	8	15.2
Poisson's ratio	0.37	0.374
Yield Strength [MPa]	18	56
Ultimate Tensile Strength [MPa]	30	106
Fracture Toughness [$kPaM^{1/2}$]	112	564

Table 1: Material primary physical properties. Compiled from [2]–[4].

A larger fracture toughness allows the structure to be lightened by removing material from the ribs by cutting holes, explained in Section 2.3.4. With balsa, a

limit would be reached relatively quickly as any cracks formed during the part's life-time would be much more likely to propagate and cause failure, due to its much lower fracture toughness.

The skin will be made from a high strength polypropylene film material; SolarSpan. This material shrinks when heat is applied, allowing it to make a taught, stiff skin with a smooth surface. This is important for aerodynamics to ensure skin friction is as low as possible. Additionally, this material is very lightweight, with an area density of only 60 to 75 gsm [5]. Although the skin is very lightweight, is will also significantly increase the stiffness of the wing structure when assembled, due to the massively increased second moment of area about the centroid.

Other small parts will be manufactured by the use of 3D printing. This allows for complex structures to be manufactured at very low cost and in a short time frame. Additionally, designs can be manufactured and then tested before being improved upon with little cost implications. Although the material selection is important, the methods of manufacture are much more influential on final part properties. This can include altering the amount and pattern of infill, as well as optimising layer adhesion by printing at hotter temperatures or altering extruder dimensions [6]. These parameters, however, can have a negative impact on other properties such as part mass and surface quality. For ease of manufacture, Polylactic acid (PLA) will be used as it has a relatively high strength and can be printed relatively easily. The tensile strength of PLA can only be matched by high performance thermoplastics such as poly-ether-ether-ketone (PEEK) [7]. This would pose large issues however, as it requires very high printing temperatures of >350 °C and a heated chamber. Use of PLA will minimise part warping to ensure dimensional accuracy.

As the fuselage has less strucutral load applied to it, styrofoam was chosen as the main construction material. Styrofoam is a closed cell polystyrene foam and has relatively poor strength characteristics. It does, however, have a very low density which is essential for ensuring the mass limit is not exceed. Additionally, it is very easily formable with basic tools so can be shaped to an aerodynamic profile with ease. It is also a very low cost material and is very easy to source.

2.2 Structure

2.2.1 Computer Aided Design

Computer aided design (CAD) is vital for the design process. A design can be laid out and then modified with the assistance of CFD and FEA processes, described in Sections 3.2 and 2.3. Using these computational methods allows the design to be iteratively improved; testing the performance characteristics and modifying certain aspects then repeating. Additionally, CAD allows the materials to be selected and mass properties to be calculated. This is useful for determining the centre of gravity in relation to the wings, to ensure the aircraft will be stable yet manoeuvrable in flight.

2.2.2 Fuselage

The design of the fuselage was highly debated amongst the group. The simpler and obvious choice would have been to go for a cylindrical/rectangular main body with a hemisphere nose. This design would have offered similar aerodynamic performance to a more sophisticated body, due to the small size of the body, whilst being much easier to manufacture later on in the project. However, it was agreed upon the whole group that a less common, more sculpted design was to be made since it would challenge our manufacturing engineering abilities as well as make the final product more aesthetically pleasable. The iterative process with all the different fuselage designs will be spoken below:

The first design for the fuselage came from the existing military surveillance UAV. This design, as seen in Figure 2 and Figure 3 was very aggressive on the nose section as it gained thickness too quickly and was in disproportion with the rest of the body. This would have created a massive separation in flow and was, therefore, rejected before any CFD analysis was even performed.

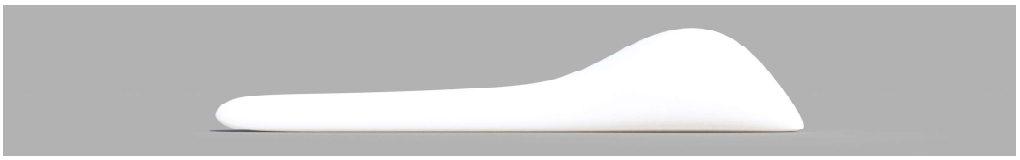

Figure 2: First iteration fuselage side view

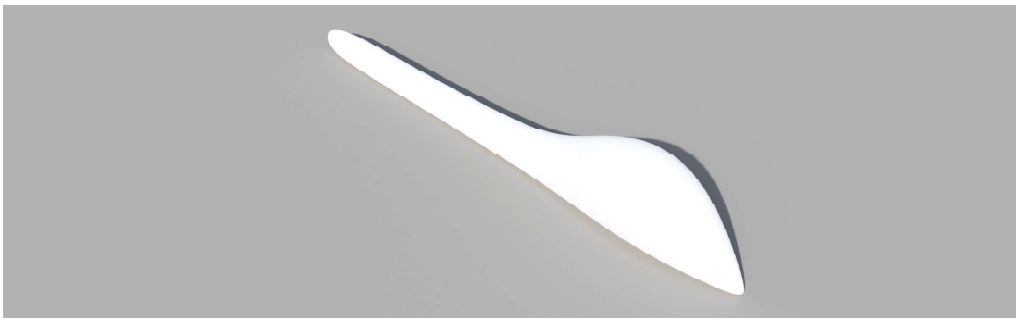

Figure 3: First iteration fuselage perspective view

The second design fuselage was very similar to the first, but had a broader rear end. This was introduced to improve the lift induced by the fuselage but was again discarded due to its complexity and poor connection with the wing and tail. There was observed to be a large separation between the rear of the fuselage and the horizontal tail piece.

Figure 4: Second iteration fuselage side view

Figure 5: Second iteration fuselage perspective view

The third design fuselage was modelled after the UCAV Kratos XQ-58 Valkyrie. This design characterized itself for having a large body resembling the hull of a boat. Although very stable and easy shape to attach the wings to, the design was impractical due to its difficulty in manufacturing as as well as the unnecessary volume. The design of the fuselage has to provide enough space in order to fit all of the avionic components, whilst minimizing the material use to reduce cost and weight. This design had enough space for the components which would be housed in the nose, but left too much at the rear.

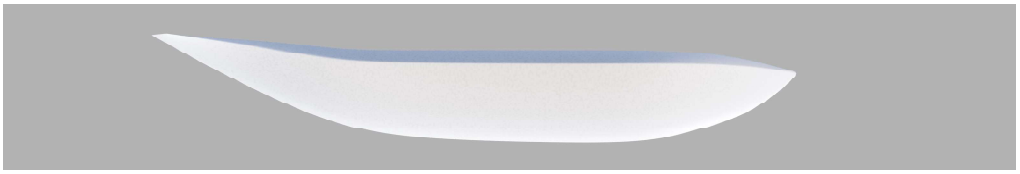

Figure 6: Third iteration fuselage side view

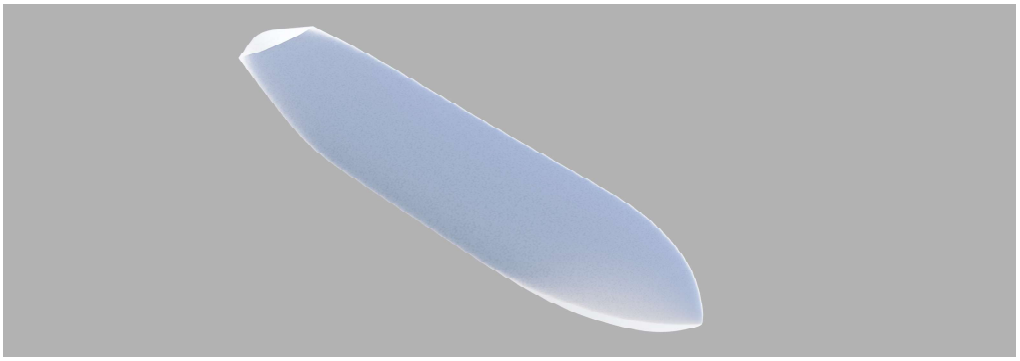

Figure 7: Third iteration fuselage perspective view

The final design came from a combination of all previous designs, the nose is the average shape obtained from all of them, whilst the rear follows the profile of [design 2] whilst maintaining the thinness and shape of [design 1]. This approach provides the perfect use of space to house the components, and at the same time reduces the overall weight, cost and material in the unnecessary areas.

Figure 8: Fourth iteration fuselage side view

Figure 9: Fourth iteration fuselage perspective view

Some readjustments had to be done in order to please the vision of the whole team, and was easily done with the form tool in Fusion 360. The top section of the body was removed and left as a flat top to more easily accommodate the wings. The shape of the fuselage provides a clear path for the tail and ensures the air flow does not negatively affect it.

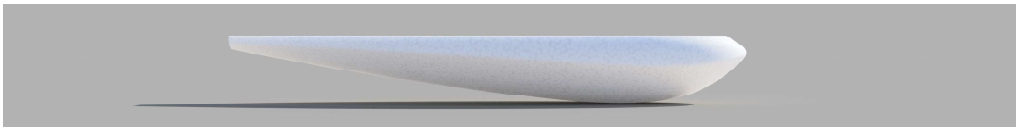

Figure 10: Final iteration fuselage side view

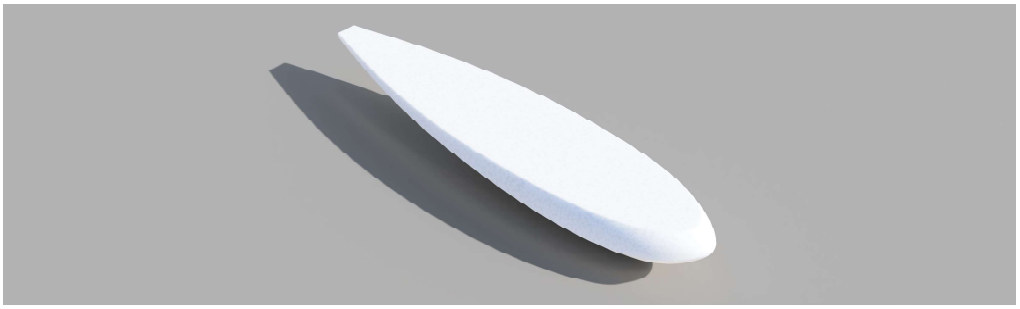

Figure 11: Final iteration fuselage perspective view

2.2.3 The Wing

A conventional rib-spar based design was used for the main wing structure. The ribs will be made from birch ply as described in Section 2.1. This allows the

main structural components to be laser cut, allowing a precise and accurate structure to be made. Two carbon spars will provide the majority of strength in the structure, withstanding the bending forces created by lift. The wing will be skinned with SolarSpan, which shrinks when heat is applied. The skin helps resist torsional stresses on the wing and also provides a smooth surface for lower skin drag.

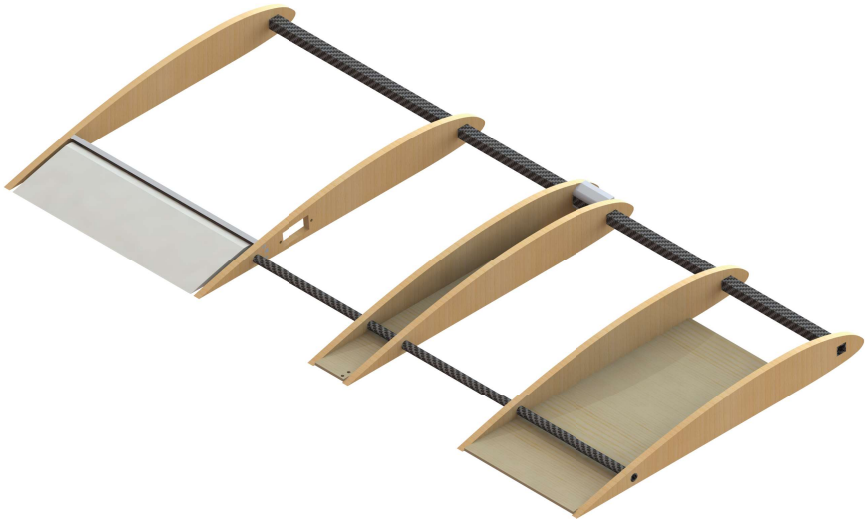

Figure 12: The initial wing structure

An initial design was produced utilizing a basic rectangular shape (Figure 12). To improve aerodynamic efficiency, a taper was added along with a small degree of twist at the wing tip. These help to produce an elliptical lift distribution which is essential for optimum flight characteristics. Additionally, twist helps the tips of the wing stall after the root. This ensures that the ailerons will continue to work even when the aircraft has begun to stall. This helps prevent irrecoverable failure such as a flat spin. The leading spar was moved backward to allow for leading edge taper. This helps reduce the load on the ribs as the spar is closer to the aerodynamic centre of the aerofoil. To improve crosswind stability, a slight 5° camber was added. This further iterated design is shown in Figure 13.

When coupled with the results from Section 2.3, this design was shown to provide the necessary strength and stiffness properties to avoid failure and meet the performance specification.

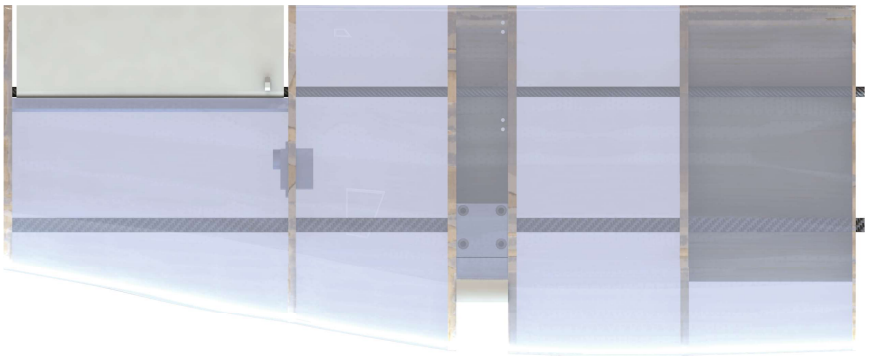

Figure 13: Iterated wing structure

The aileron shape was based on the aerofoil profile shape, ensuring maximum aerodynamic performance (Figure 14). The use of 3D printed manufacturing allows a complex geometry to be designed, leaving a small gap between the wing skin and aileron. This minimises drag lost at this intersection. In order for the aileron to have smooth, consistent motion, the aft spar is used as a hinge. This allows the aileron to rotate about this axis and ensures the wing strength is not compromised over the span. A simple bushing is used as opposed to a bearing due to space and mass restrictions, although friction is this system will be negligible. The pushrod arm for the aileron has multiple mount points to allow the throw distance to be adjusted in the field if control authority is not correct.

Figure 14: Cross-section of the aileron structure

2.2.4 The Tail

For simplicity, the tail will be made from a thin, flat plate. This allows aerodynamic properties to be easily estimated using thin aerofoil theory; $c_l \approx 2\pi\alpha$, where α is angle of attack. As the tail is only to provide a correction to the

main wing's pitching moment, its aerodynamic properties are not essential and optimizing structural integrity dominates. A flat plate will provide sufficient lift at low drag while ensuring the tail is stiff and lightweight.

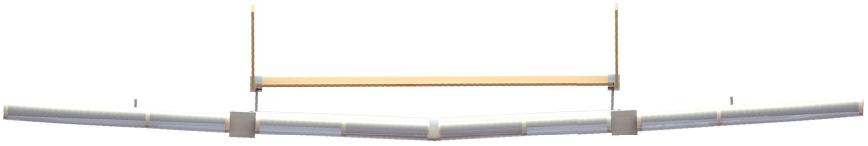

Figure 15: Front-top view of the wing structure showing the tail configuration

The tail is design around a twin boom configuration, utilizing two vertical rudders. These are placed behind the motors, allowing the propeller wash to improve control authority due to the increased airspeed. The tail can also strengthen the wing as it acts as an additional horizontal spar, creating a triangular shape with the dihedral (Figure 15).

Centre of Mass Adjustment Allowing the centre of gravity location to be moveable poses a large advantage as adjustments can be made in the field to alter flight characteristics. To cater for this, the tail booms are mounted on adjustable clamps (Figure 16). If the centre of gravity is in the incorrect location, these clamps can be adjusted to allow the tail to be moved relative to the main wing.

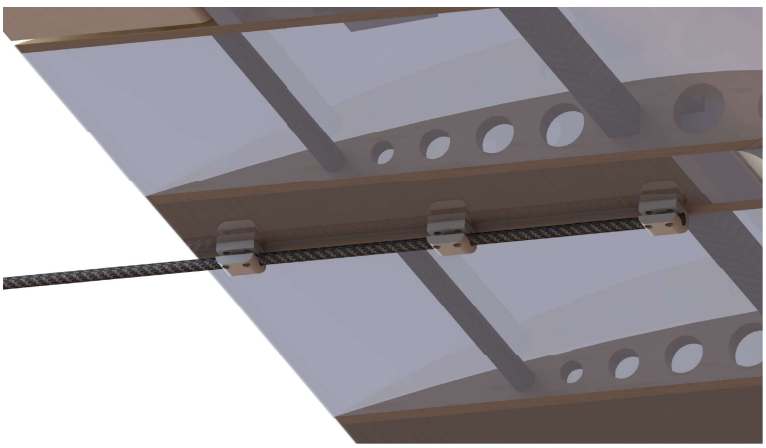

Figure 16: Adjustable clamps to adjust centre of gravity by moving the tail

2.3 Finite Element Analysis

As the most important part of our UAV, wing is responsible for generating lift, so the analysis of the wing is of great importance. However, during the flight of the UAV, the flight environment is complicated and constantly changes. The upper and lower pressure, the aerodynamic lift and drag, would vary when the flow field around the wing changes. As a result, the wing structure would produce flexure deformation, and it may threaten the stability and safety of flight and even lead to the failure of mission. To avoid this, its reasonable to predict the performance of the wing using finite element analysis.

The Finite Element Analysis (FEA) is the simulation of real physical phenomenon using the numerical technique called Finite Element Method (FEM). In a real physical phenomenon, several process may happen, including physical, thermal, and electrical process. Theoretically, these process can be predicted by solving their governing equations, usually partial differential equations (PDEs). The principle of the FEM is: cut the continuous real system into several elements, and with the finite element and nodes, the computer can calculate the outcome. Consequently, the outcome is a simulation of the real physical phenomena.

In this paper, the finite element analysis is based on the ANSYS WORKBENCH 18.2. First, static structure analysis is carried out to find the wings performance under load. Second, aim at the wing model, modal analysis is done for the vibration measurement and dynamic analysis. Finally, the deformation of the wing during the flight can be obtained through transient structural analysis. With all these works done, a comprehensive and in-depth understanding of our groups wing model can be obtained. Our group choose NACA 3310 as our airfoil, and our wing model consists of thin skin, double spars and several ribs, as Figure 17 shows.

	Plywood	Carbon Fiber T300	Polypropylene
Density $[kg/m^3]$	748	1750	91
Young's Modulus $[Pa]$	$6.32e9$	$2.37e10$	$8.9e8$
Poisson's Ratio	0.25	0.21	0.42
Tensile Yield Strength $[Pa]$	$3.81e7$	$3.53e9$	$3.28e7$
Tensile Ultimate Stregth $[Pa]$	$5.61e7$	$3.75e9$	$3.60e7$

Table 2: Properties of the materials.

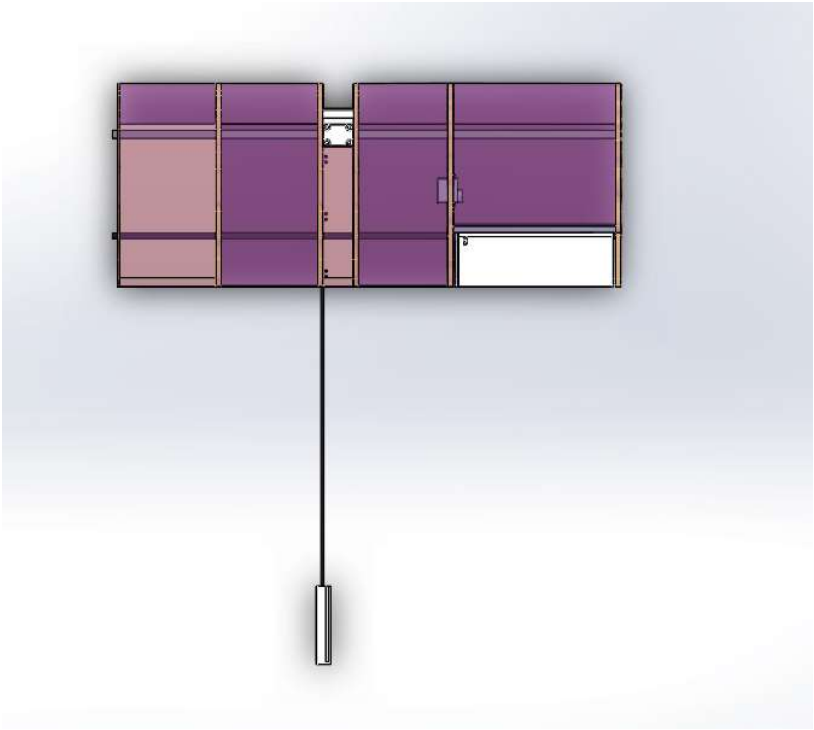

Figure 17: Wing model

As to the material, we choose plywood for ribs, carbon fibre T300 for spars, and. The properties of the materials are as Table 2.

2.3.1 Static Structural Analysis

Model By using the mesh tool of ANSYS and adjusted several parameters, a reasonable mesh is generated as in Figure 18.

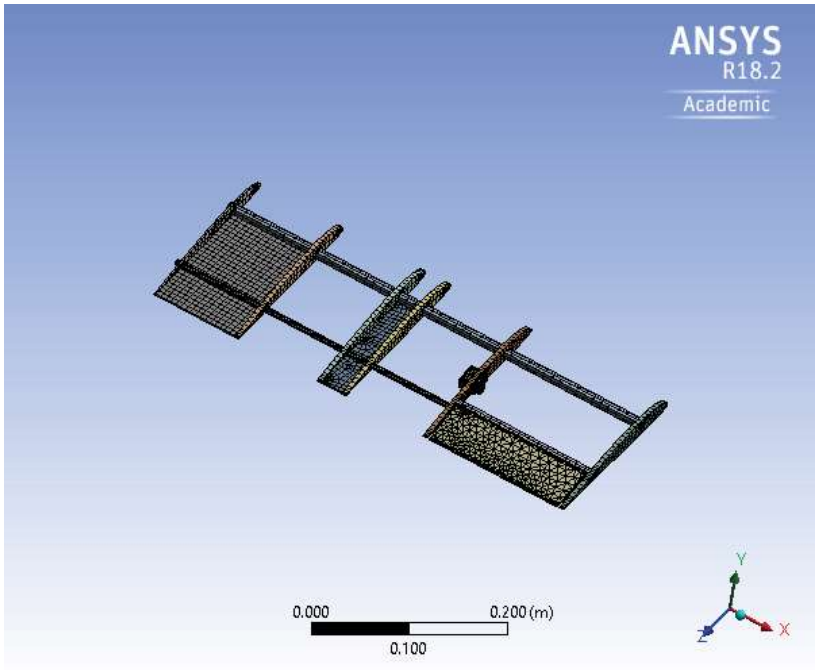

Figure 18: Mesh of the wing structure

Boundary conditions To analyze the deformation and load condition of the wing structure during its flight , fixed support is added to the surface which the wing is attached to the fuselage. And an upper stress of $1e5Pa$ is added on the top surface of the wing structure.

Outcome After finishing mesh and setting boundary conditions, the software can calculate the simulation results for us.

Total deformation Figure 19 is the outcome of the total deformation, the deformation of the wing structure increases along the direction of the wing span, and reaches the maximum at the wingtip, the value maximum total deformation is 0.0497m.

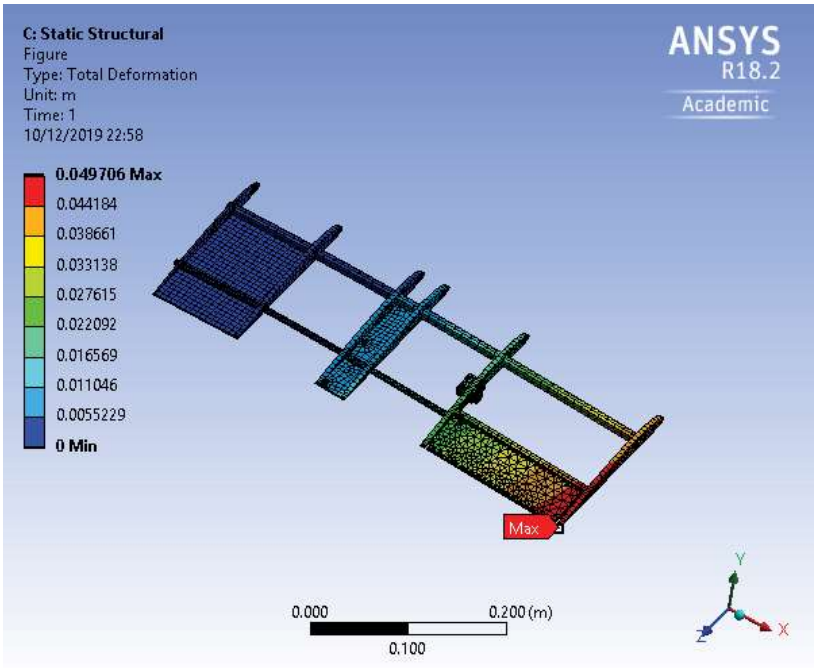

Figure 19: Total deformation of the wing structure

Equivalent stress Figure 20 is the outcome of the equivalent stress (von-Mises stress). The equivalent stress on the ribs is relatively small, the two spars bear more equivalent stress. By using the max pin, the maximum equivalent stress can be found at the connection part of the thinner spar and the rib, and its value is 1.12e9 pa, that may be dangerous for the structure.

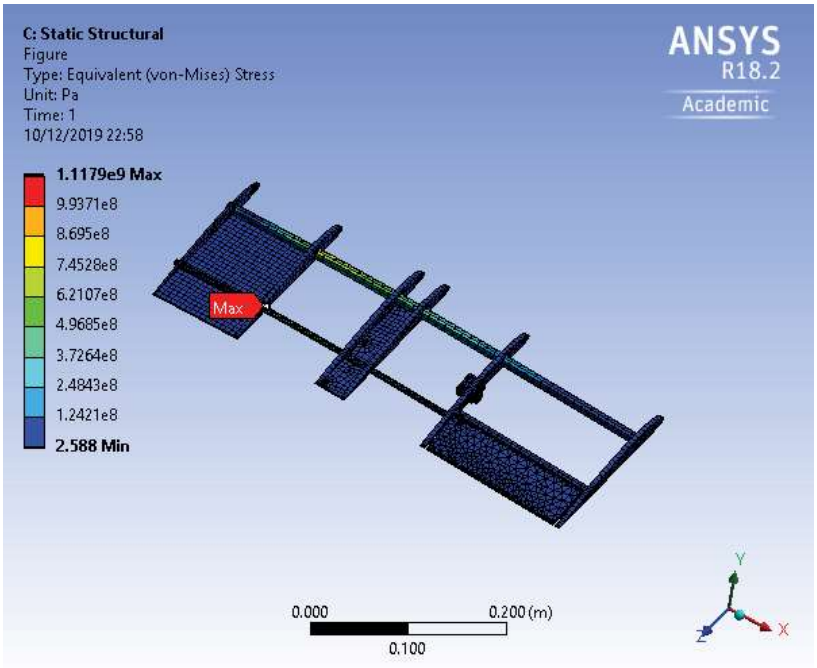

Figure 20: The equivalent (von-Mises) stress

Safety factor The safety factor in ANSYS is defined as the ratio between the strength of the material and the maximum stress of the structure in this part. When the stress in the structure is smaller than the strength of the material, the safe factor is up to 1 and the structure is safe. From figure 21 we can find that most part of the wing structure is safe. However, some connection part of the wing structure is weak, especially the one in the top left hand corner, the safety factor in the middle part of the two spars is also small. In the building process, these position should be strengthened.

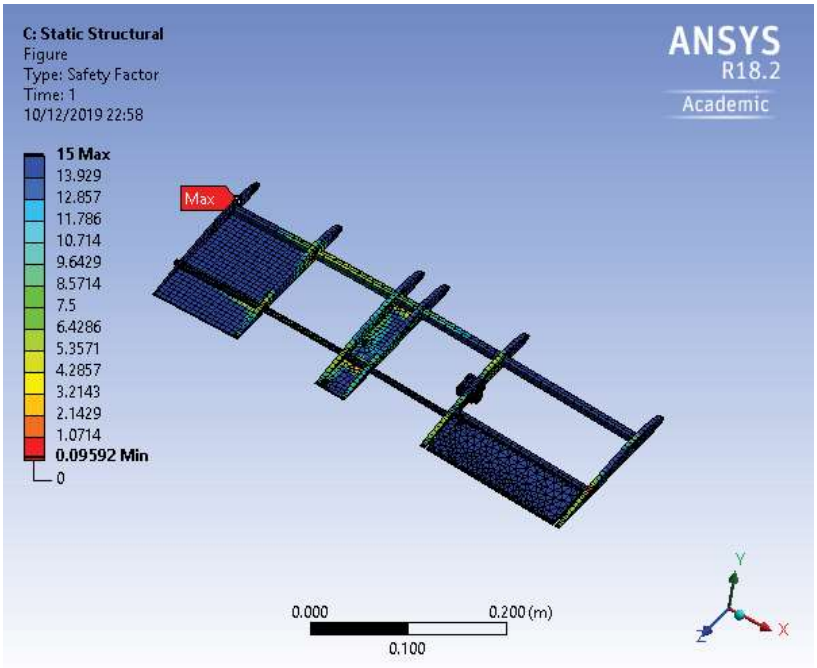

Figure 21: The safety factor of the wing structure

2.3.2 Modal Analysis for the Wing

Modal analysis During the flight, flutter is an unstable vibration of an elastic body in the air flow. And the flutter of the aircraft is a kind of self-excited vibration caused by the coupling of the elastic force, inertial force and aerodynamic force on the wing [8]. Once the flutter happens to the aircraft, it will cause unavoidable structural destruction. Mode is the inherent vibration characteristic of mechanical structure, and modal analysis is the way to study the modes. Each mode has specific natural frequency, and modal shape. In usual conditions, the wing structures vibration is the superposition of several modal shapes. When the frequency of the wing structure is near one specific natural frequency, the modal shape of this natural frequency would play a leading role. By modal analysis, we can effectively prevent the aircraft from the flutter.

Mesh By using the mesh tool of ANSYS and adjusted several parameters, the mesh of the wing is generated as in Figure 22

Order	Frequency [Hz]	Modal shape
1	47.245	Bending
2	169.91	Torsion
3	215.53	Bending
4	231.23	Bending
5	331.67	Bending
6	341.17	Bending

Table 3: Results of modal analysis.

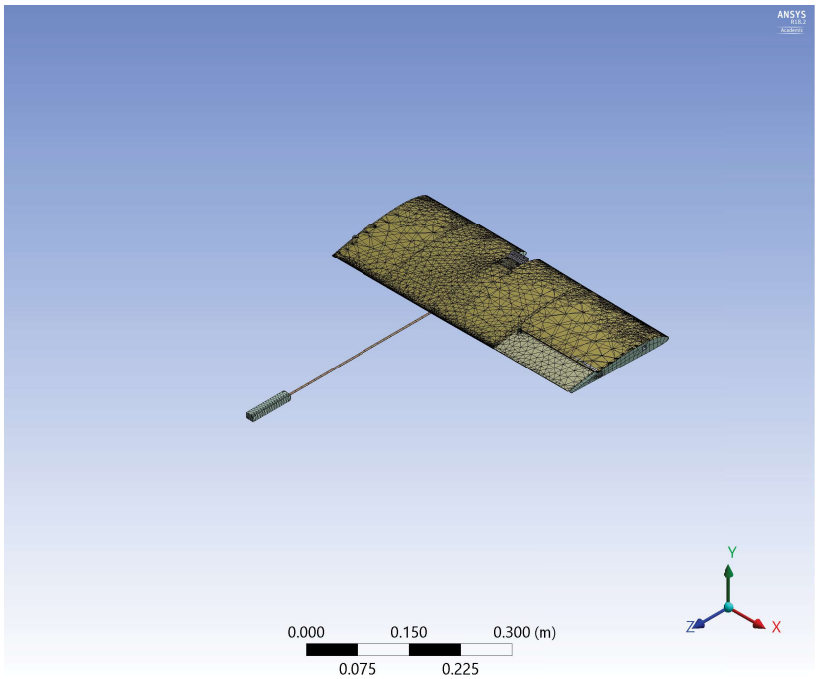

Figure 22: Mesh for modal analysis

Boundary Conditions Fixed support is set where the wing is attached to the fuselage, and also the tail.

Natural Frequency After meshing and setting boundary conditions, the software can calculate the first six natural frequencies of the wing structure, as in Table 3.

Modal Shape The modal shape of the first six orders is depicted in Figures 23a-23f

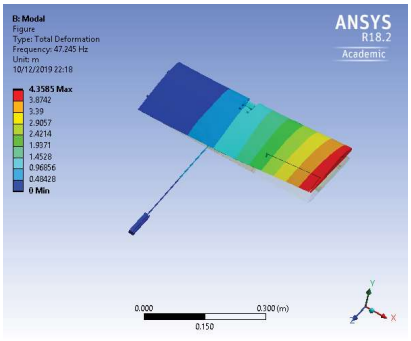

(a) First modal shape

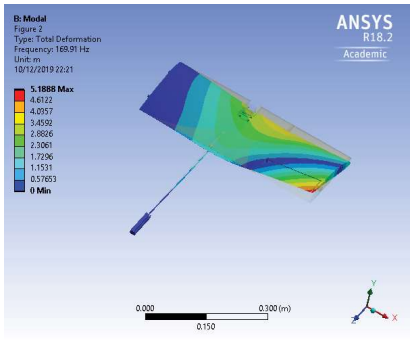

(b) Second modal shape

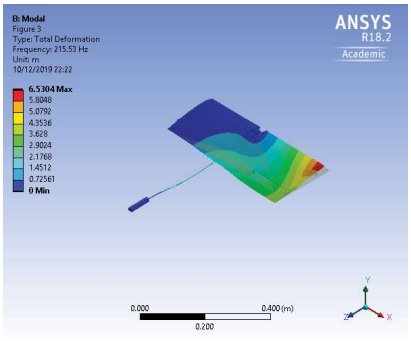

(c) Third modal shape

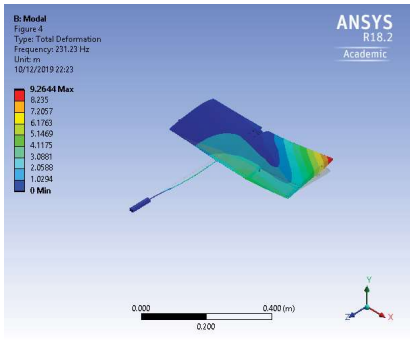

(d) Fourth modal shape

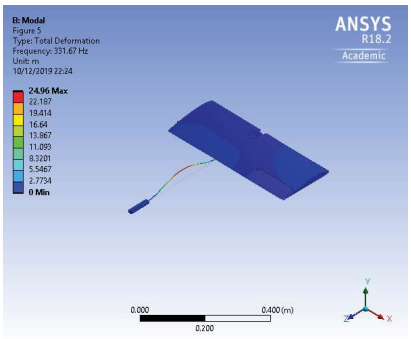

(e) Fifth modal shape

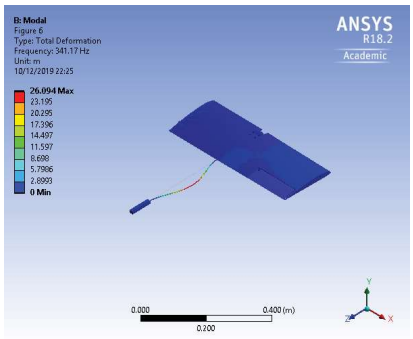

(f) Sixth mode shape

As is shown is the analysis results, there are both bending and torsional deformation in the modes of the first six orders. In the modal shapes of the four orders except the second, the wing mainly produces the bending deformation. However, the modal shape of the second order changes obviously, which becomes the torsional deformation. In addition, the deformation increases along the direction of the semispan, and reaches the maximum at the wingtip. In the first four mode, the deformation is mainly about the wing, and in the fifth and

sixth mode the spar between the wing and tail deform mostly. Looking at the inner structure as Figure 24 shows, we may find that the spars mainly bear the bending deformation, and the skin and ribs mainly bear the torsional deformation.

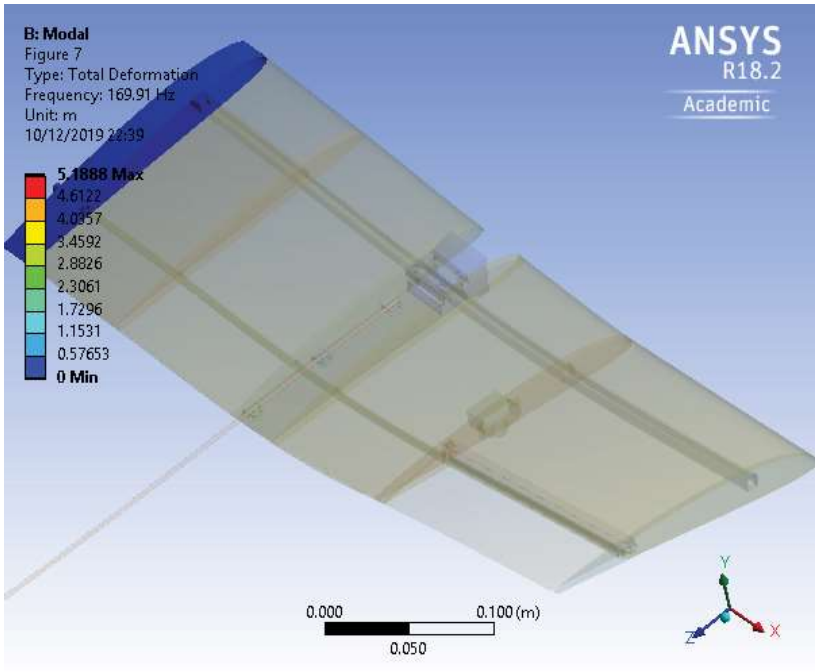

Figure 24: Inner structure

As a result, when the frequency of the wing is close to the natural frequencies of the first four orders except the second one, the spars of the wing should be strengthened. When the frequency of the wing is close to the natural frequency of the second mode, the wing will suffer the torsional deformation, and the serious change of the aerodynamic characteristics caused by the huge shift of the modal shape may lead to a flutter. Therefore, if the frequency is close to the natural frequency 169.91Hz, it's necessary to improve the design of the aircraft in order to avoid this kind of deformation.

2.3.3 Transient structural analysis for the wing

Transient structure analysis After modal analysis, the natural frequencies of the wing are obtained. And the higher the modal order is, the higher the natural

frequency is. During the flight, the frequency of the wing caused by the external disturbances is closer to the low- order frequency [9]. Therefore, it's reasonable to consider only the modes of the first three orders in the transient structural analysis. Transient structural analysis is a method applied to determine the dynamic response of the time- varying loads, and is also called time-history analysis [10]. This method can be used to calculate the time-varying displacement, stress and strain of the structure subjected to the time varying loads.

Load Setting During the flight, the wing is mainly subject to the gravity and aerodynamic loads. The wings deformation and local stress changes with the varying distribution of the aerodynamic loads. Through the transient structural analysis, the deformation data of the wing can be obtained. As the primary external forces of the wing, the aerodynamic loads are distributed evenly on the skin, because our wing model is the straight wing. By arranging an equivalent strain bridge, the relationship equation between load input and strain output could be established, and the load-time relationship was obtained [9]. To simulate the launch of the missile, the load force is set as 1000N in the initial time, and start decreasing after the first 0.01s, finally reach 0N at 0.2s, as in Figure 25.

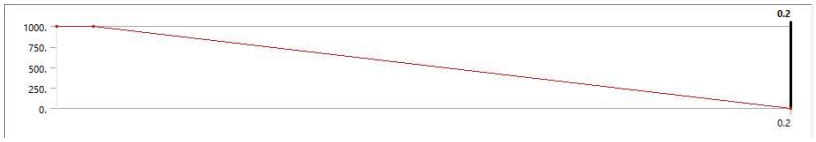

Figure 25: Load force

Outcome After the transient structure analysis, we may obtain the deformation and stress of the wing structure in the 0.2s. Figure 26 and Figure 27 shows the total deformation and equivalent (von-Mises) stress of the wing structure at 0.2s.

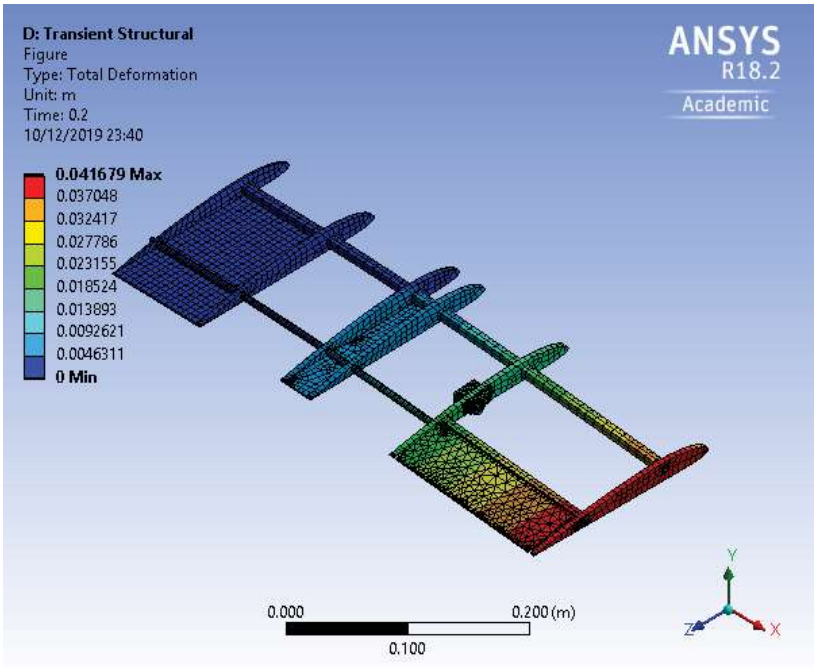

Figure 26: Total Deformation

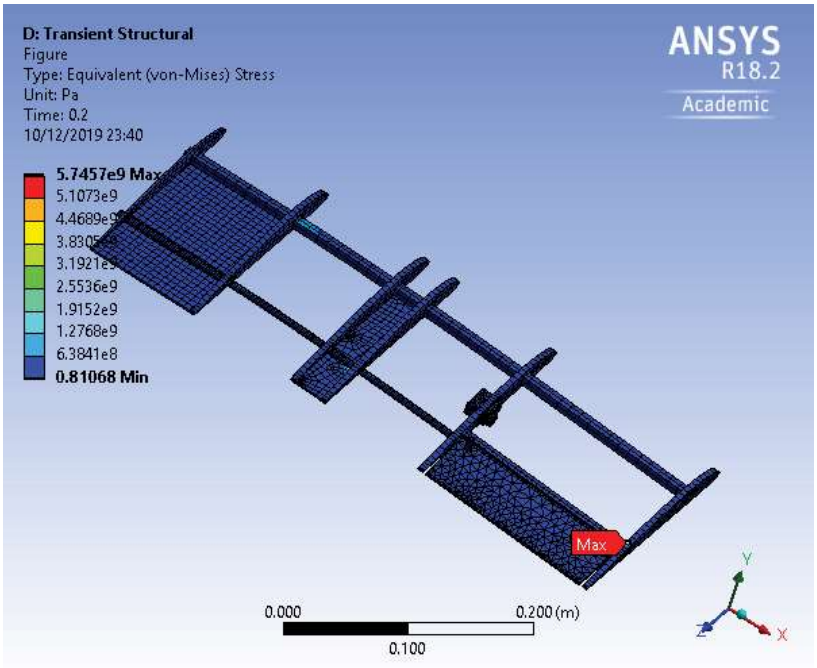

Figure 27: Equivalent (von-Mises) Stress

Figures 28 and 29 show the total deformation and equivalent stress change in the 0.2s, Table 4 shows their specific value.

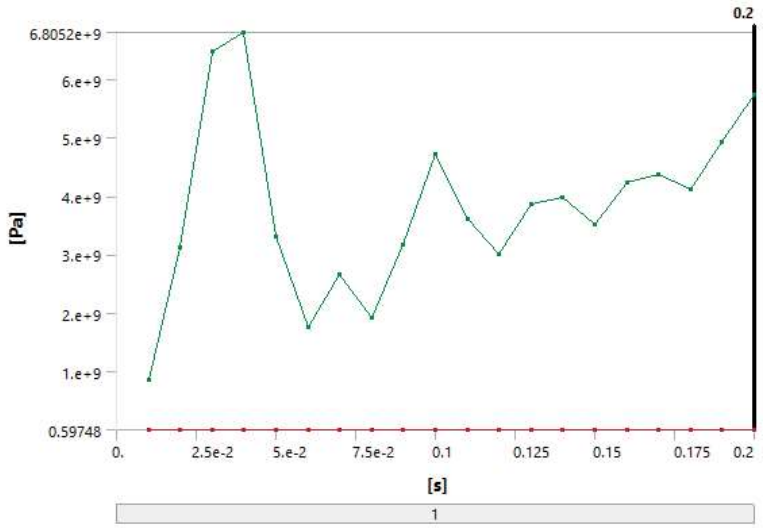

Figure 28: Pressure change in the 0.2s

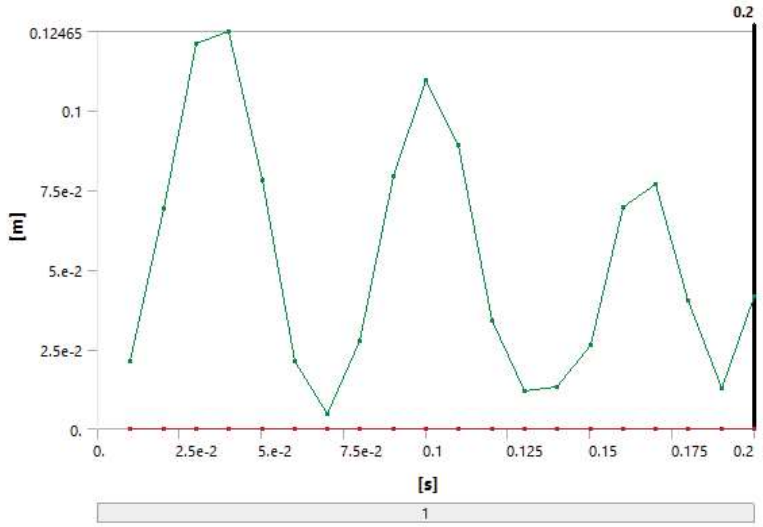

Figure 29: Total deformation in the 0.2s

The total deformation in the 0.2s has 3 cycles, the peak value of the first cycle is the highest, with the value of 0.12465m , and the peak value of the second cycle and third cycle decrease by degrees. However, the equivalent stress in the 0.2s has 5 cycles, the peak value of the first cycle is the highest. The first peak value is 6.8e9 Pa at 0.04s, the same time as the first peak value in total deformation, making this time the most dangerous point in the 0.2s. After that, the peak value of the equivalent stress drop to the lowest and then increases. The

Time [s]	Total deformation [m]	Equivalent [Pa]
0.01	$2.1107e-2$	$8.6621e+008$
0.02	$6.9215e-2$	$3.1271e+009$
0.03	0.12104	$6.4805e+009$
0.04	0.12465	$6.8052e+009$
0.05	$7.7809e-2$	$3.3182e+009$
0.06	$2.1177e-2$	$1.7506e+009$
0.07	$4.8471e-3$	$2.6584e+009$
0.08	$2.7583e-2$	$1.9212e+009$
0.09	$7.935e-2$	$3.1802e+009$
0.10	0.10942	$4.7274e+009$
0.11	$8.9125e-2$	$3.6206e+009$
0.12	$3.3836e-2$	$3.0182e+009$
0.13	$1.1678e-2$	$3.8746e+009$
0.14	$1.3323e-2$	$3.9925e+009$
0.15	$2.641e-2$	$3.51e+009$
0.16	$6.9682e-2$	$4.2262e+009$
0.17	$7.6943e-2$	$4.3775e+009$
0.18	$4.0284e-2$	$4.1152e+009$
0.19	$1.2742e-2$	$4.9197e+009$
0.20	$4.1679e-2$	$5.7457e+009$

Table 4: Total deformation in 0.2s.

vibration is not one specific mode, but the combination of several modes.

2.3.4 Rib Structural Analysis

One important area of the design to reduce weight is the ribs in the wing. This is because a strong but dense material was selected for their construction. This allows holes to be cut in order to remove mass in the optimal locations.

As the rib model is relatively small, a mesh could be created with high density to maximise result accurracy without performance penalties (Figure 30). When a mesh skewness analysis is run, no errors are generated. This means the mesh is of sufficient quality to produce accurate results.

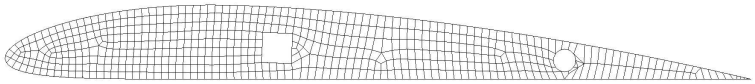

Figure 30: Automatically generated mesh

Using the CFD analysis, forces on the wing at an angle of attack of 15° and velocity of $20\,\mathrm{ms}^{-1}$ were transposed onto a main wing rib from the pressure distribution. A relatively high angle of attack was used as this will maximise the forces applied to the wing while staying in a reasonable flight envelope. Boundary conditions were applied in order to constrain the model at the spar connections.

Material Properties were taken from Section 2.1, using properties for birch plywood.

Once a stress analysis was performed on the rib with no mass optimization, holes were cut out of the profile to remove material. Stress analysis was then performed again before altering the dimensions of the holes. After multiple iterations, a final geometry was chosen and analysed (Figure 31).

The results show an equivalent peak maximum stress of 2.25 MPa, located near the aerodynamic centre at approximately 25 % of chord. This is a significant margin lower than the yield stress of the material; 56 MPa. Although there is a large safety factor, the holes will not have increased size as this will increase

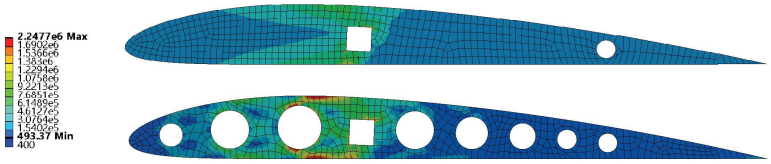

Figure 31: Equivalent (von-mises) stresses on the rib before and after mass optimization. Scales matched.

their chance of failure via fracture.

Using Equation 1, a critical crack length, a_c, of 1.68 mm was calculated, using a fracture toughness, K_{IC}, from Table 1.

$$K_{IC} = C\sigma\sqrt{\pi \cdot a} \tag{1}$$

(Where $C = 1.12 - 0.231\left(\frac{a}{W}\right) + 10.55\left(\frac{a}{W}\right)^2 - 21.72\left(\frac{a}{W}\right)^3 + 30.39\left(\frac{a}{W}\right)^4$)

This simplifies the system to a through-thickness edge crack at the thinnest part of the structure, whose width, W, is 3 mm. Any crack larger than this would result in failure during flight. However, this only concerns the maximum stress in flight conditions. In the event of a crash or hard landing, peak stresses reached could be much higher. With a crack length of 0.05 mm, a critical failure stress, σ, of only 11.0 MPa was calculated. A crack this small could easily form during the manufacture process and may not be noticed. Because of this, the thinnest part of the rib was limited to 3 mm and parts will be meticulously visually checked prior to final assembly and flight.

The result of rib optimization allowed the mass of each rib to be reduced by 1.8 g. This corresponds to a total mass reduction of ~20 g over the whole wing. Although a relatively small reduction, this will still improve performance of the aircraft with little downsides.

3 Aerodynamics

3.1 Aerofoil Selection

The aerofoil section choice for the main wing is greatly important as it is the basis for the aerodynamic characteristics of the aircraft. To simplify the process, only 2D conditions would be considered when choosing the aerofoil shape. This means discounting any flow in the spanwise direction.

The design criteria was used to define the conditions used to find the most efficient and effective aerofoil in cruise. Cruise performance is the most relevant as the aircraft will spend the majority of the flight in cruise conditions.

From this, the weight of the aircraft was considered to be the maximum allowable; 1.5 kg, giving a required lift of $L_{cruise} = 1.5 \times 9.81 = 17.72\,\text{N}$. The wing span was also defined as the largest allowable; 1 m. Cruise airspeed was estimated to be 20 m/s. Using Equation 2, it can be seen that there are two unknown variables; S, wing surface area, and the aircraft coefficient of lift, $C_L^{(a/c)}$.

$$C_L = \frac{2L}{\rho V^2 S} \tag{2}$$

To solve this, wing area was assumed to be 0.2 m, which gives a chord of 0.2 m. This dimension was gathered from historical designs of various remote control planes of this size. The required lift coefficient of the aircraft can then be calculated to be 0.300. This however, does not consider losses due to 3D flow or fuselage lifting effects. To rectify this, the required lift coefficient of the aerofoil, $C_{L_{cruise}}^{(foil)}$, is calculated with Equation 3.

$$C_{L_{cruise}}^{(foil)} = \frac{C_{L_{cruise}}^{(a/c)}}{0.95 \times 0.9} \tag{3}$$

A final lift coefficient for the aerofoil can then be determined to be 0.351.

To decide on a section profile, a Python program was written to automate

XFOIL, a program to determine pressure distributions over an aerofoil in given conditions. This utilized the Python `xfoil` library [11]. Every National Advisory Committee for Aeronautics (NACA) 4-digit aerofoil with a thickness greater than 10 % of chord was tested at the defined $C_{L_{cruise}}^{(foil)}$. The selection was limited to 4-digit aerofoils for simplicity and because XFOIL can only perform calculations on some 5-digit foils. Additionally, some 5-digit aerofoils contain reflex curves which would make applying the skin much more difficult or impossible during the manufacturing process. Thickness was limited as any thinner aerofoils would not allow large enough spars to be used for a sufficiently strong wing structure. The aerodynamic efficiency, L/D was determined for each aerofoil. The best performing aerofoils are shown in Table 5.

Aerofoil	C_L / C_D
3310	45.65
2410	45.58
1510	45.45
1610	45.35
2310	45.31
3410	45.05
1410	44.86
2210	44.45
1810	44.13
1710	44.12

Table 5: The ten best performing NACA aerofoils at $C_{L_{cruise}}^{(foil)}$

It can be seen that the variance in performance between the aerofoils is minimal, indicating that any could be suitable for the task. To further determine the most suitable foil, the best six were plotted (Figure 32).

This shows that, while performance at cruise is almost identical, performance in other flight conditions is variable. The NACA 1510 and 1610 foils show very poor performance at larger values of C_L, stalling at a low value of ~1.4. When comparing NACA 3410 and 3310, the former shows a better aerodynamic efficiency in larger lift regions, however a further aft camber is disadvantageous for structural reasons. A maximum camber near the aerodynamic centre of the aerofoil is desirable as it gives more space for a spar to be inserted

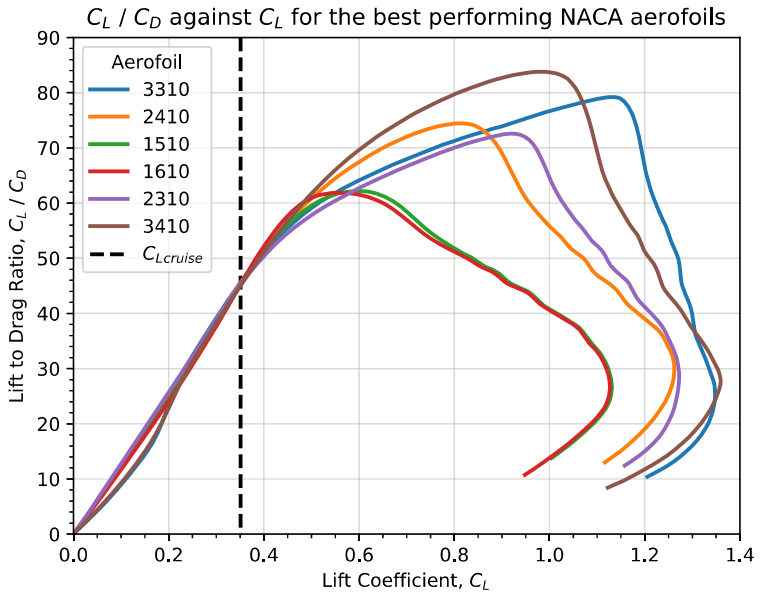

Figure 32: XFOIL Prediction of lift to drag ratio of the best performing aerofoils. The vertical line indicates C_L at cruise. $Re = 2.64 \times 10^5$

in an ideal location, allowing a stronger rib. The aerodynamic centre is located at ~25 % of chord, from thin aerofoil theory. For these reasons, the NACA 3310 aerofoil was be chosen for the main wing.

3.2 Computational Fluid Dynamics

3.2.1 Introduction

In order to validate the design and ensure enough airflow flows over the control surfaces a computational fluid dynamics (CFD) simulation was run on the aerofoil, the fuselage and finally the entire aircraft. The CFD simulation also allows for the determining of the lift and drag generated by the aircraft in order to help calculate the thrust required by the aircraft at cruise or varied angle of attack conditions. CFD solvers are based on the finite volume method where the domain is discretized into a finite set of control volume, the general conservation equations for mass, momentum and energy are then solved on this set of control volumes. These equations are known as the Navier-stokes equations which have

no analytical solution for the general case [12].

3.2.2 Geometry

Before any calculations could be run, the geometry and mesh had to first be made. In order to create the geometry, the part was firstly created in CAD and imported. In order for the 3D CAD model to be imported successfully into CFD, the CAD file was saved in an IGES format.

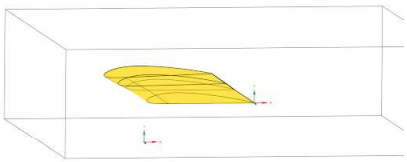

Figure 33: Geometry used for the wing, with the aerofoil highlighted.

A 3D approach was decided upon for all bodies, as none of them are uniform across their length. Also, using 3D geometry provides an analysis that's more similar to a real life situation, allowing for end effects, therefore, providing a more accurate result.

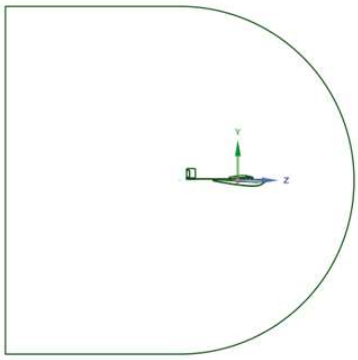

Figure 34: Side profile of the geometry used for the full body simulation.

The SpaceClaim software integrated within Ansys was used in order to create the geometry for each part. All the geometries were first created on a 2D plane along the central axis of the model, and then the pull tool was used to encase the part. At which point the part was subtracted from the created solid, allowing for the simulation of airflow around the part. For both the fuselage and

aerofoil geometry, a cuboid was used. This mesh was chosen due to the fact only a 0 degree angle of attack simulation was chosen to run on these parts, as they were mainly used as validation for the full body mesh as well as an estimation for thrust calculations. For the full aircraft simulation, a C-mesh was used so that the velocity vector could be easily changed in order to simulate different angles of attack without having to remake the entire mesh. The CAD models also had to be simplified as the geometry was too complex to create an effective mesh, therefore the CFD simulation is an approximation based on a simplified model. In addition, as all the parts are symmetrical about the central axis, symmetry could be used within the calculation in order to allow for a finer mesh across half of the part while simultaneously reducing the total time needed to run the CFD simulation [13].

3.2.3 Meshing

After the geometry had been completed, a mesh was created. Due to the complicated geometry involved within the parts, auto generated meshes were used.

Figure 35 shows an example auto-generated mesh for the full body without any other constraints applied. In order to improve the simulation, an inflation layer was applied to the surface of the part, as well as defining the surface of the part as hard. This means that the contours of the part were followed as accurately as possible by Ansys, the mesh was then re-generated.

These constraints allowed for relatively accurate values of lift and drag to be found while simultaneously not taking too long to perform the simulation. A finer mesh could be used for the simulation; however, then the calculation would take more time due to requiring a larger amount of processing power whilst not yielding a significant change in result, therefore the mesh used is a good approximation.

This is of great significance to larger simulations as a finer mesh can require a calculation to require a much larger amount of processing power, and change the calculation time from a matter of days to a matter of weeks.

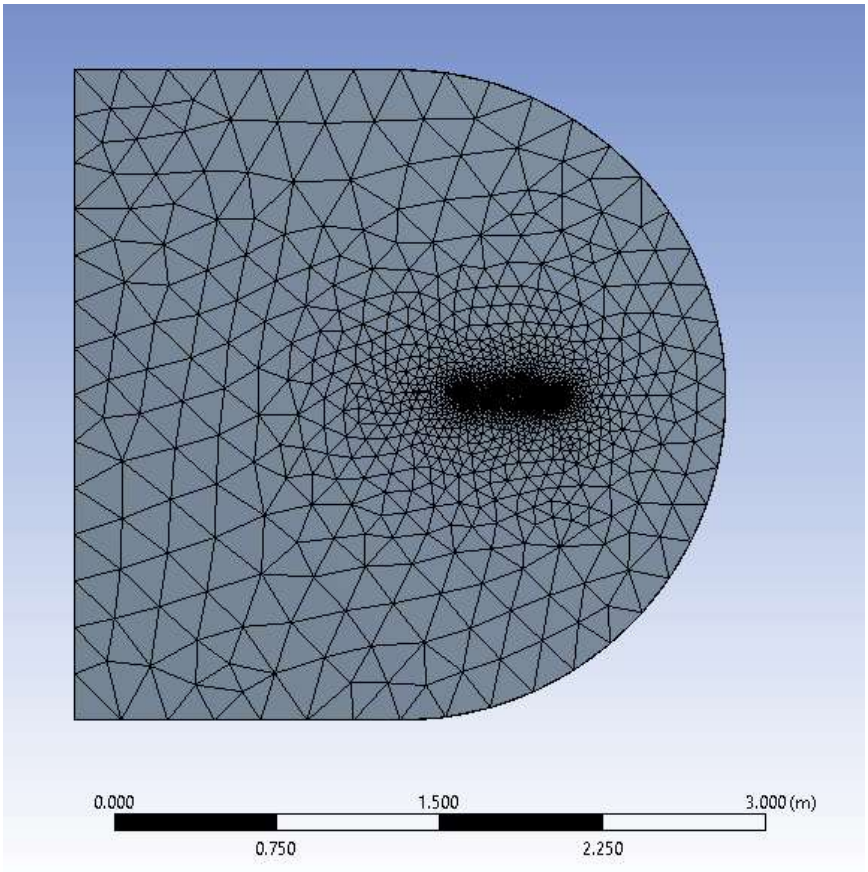

Figure 35: Auto-generated mesh for the full body simulation

Before the calculation was run, the faces first had to be defined by naming them. All meshes contained an inlet, an outlet and a plane of symmetry.

The symmetry defines a plane of symmetry allowing for an analysis of a full model while using a half body. The inlet is the position in which the fluid flow is created in the simulation. The outlet is defined as a pressure outlet, and provides a location for any airflow to leave the simulation. This helps to reduce the time needed for the calculation to be run, while also allowing for a better mesh to be applied to the half body. The plane section shown in Figure 37 is the surface created by subtracting the half plane, and is named so that it can be used to calculate the lift and drag acting on the body. This method was used for all of the simulations. Any surface not highlighted is defined as a wall within Ansys, which means airflow cannot pass through it [14].

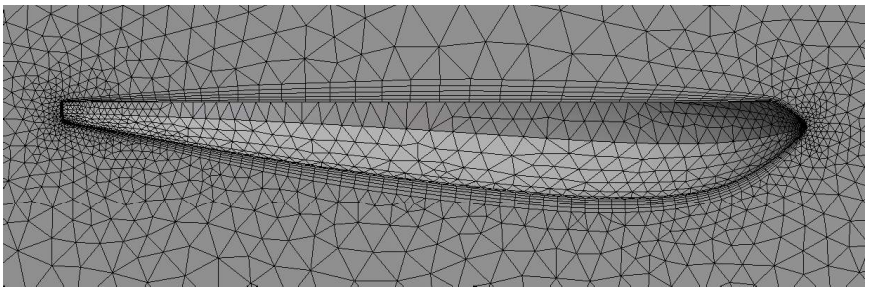

Figure 36: Mesh for the fuselage with an inflation layer and hard sizing applied.

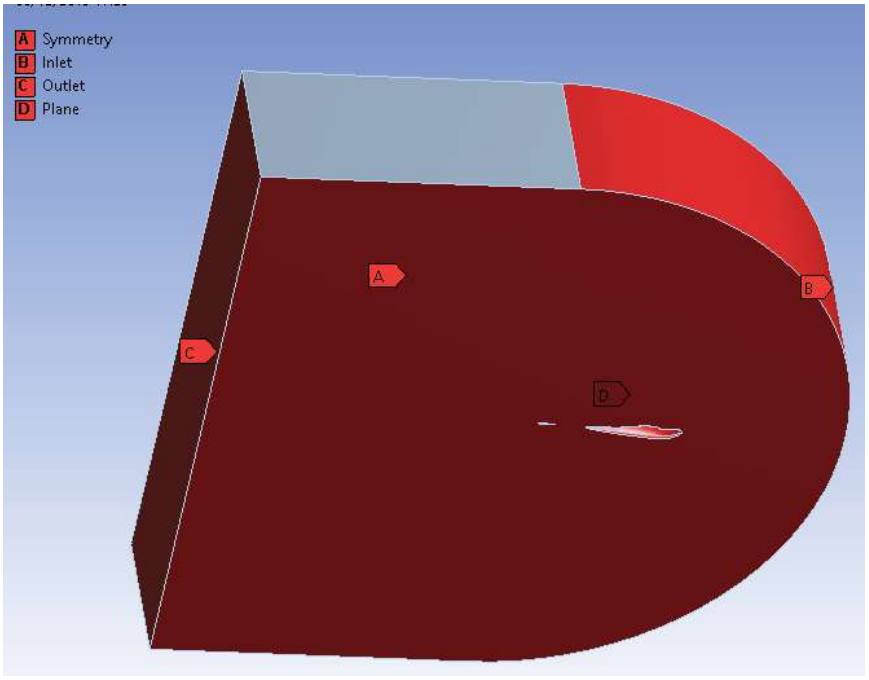

Figure 37: Named sections for the full model simulation

3.2.4 Calculation

In order to run the calculation, the appropriate conditions need to be set up to provide the data required. Due to the relatively low flying speed of the UAV, it has a very low Reynolds number, therefore the laminar model is a suitable approximation for all simulations ran. After the appropriate model had been selected, the correct material properties must also be set; in this case, the material properties for air at sea level were used. Next the boundary conditions needed to be set, using the named sections previously created, the inlet needed to be set as a velocity inlet, while the outlet must be set as a pressure outlet. The symmetry also needed to be set as a symmetry, and finally all other named sections were

set as interiors and walls. A velocity of 16 m/s was initially applied to both the wing and fuselage using an estimation of cruise speed, this was done using components where it was purely in the negative z-direction In the case of the full body, a velocity of $20\,\mathrm{m\,s^{-1}}$ was applied, where it was purely in the negative z-direction at 0 degrees angle of attack, and using $Z = -20\cos\alpha$ and $Y = 20\sin\alpha$ for the Z and Y components at any other angle of attack. For all simulations, the coupled scheme was used, with momentum set to second order upwind, all other settings were left as their defaults. Monitors were then set in order to determine when to end the calculation. An absolute criterion of 1×10^{-6} was set for the residuals meaning that if the calculated value changes by more than this value, the solution has not converged, whereas if it changes by less than this it has converged and the calculation is halted. Plots for the lift and drag force were created for all 3 simulations so that each respective value could be found. The solution was then initialized using hybrid initialization, after which the calculation was run until convergence.

3.2.5 Wing

CFD was first run on the wings in order to determine the flight speed to obtain 15 N of lift, whilst also determining the drag at this condition. It was found, that originally a speed of around 16 m/s was needed for the wings to provide enough force to counteract a UAV at the maximum weight of 1.5 kg. In this simulation, a lift force of 15 N was generated, whilst a drag force of 0.375 N was generated.

Figure 38 shows the velocity streamlines over the aerofoil, this figure shows an increase in velocity over the top of the wing, which as such leads to a decrease in static pressure, generating lift.

Figure 39 shows that the airflow re-combines at the end of the aerofoil, leading to a reduction in separation and drag generated. In addition, the 3D model doesnt appear to show any vortices which is good for the design as this also results in a reduction of drag compared to a model with vortices.

The wing simulation was mainly used in order to estimate a speed to run the full body simulation in. In addition, the wing simulation validates the selection

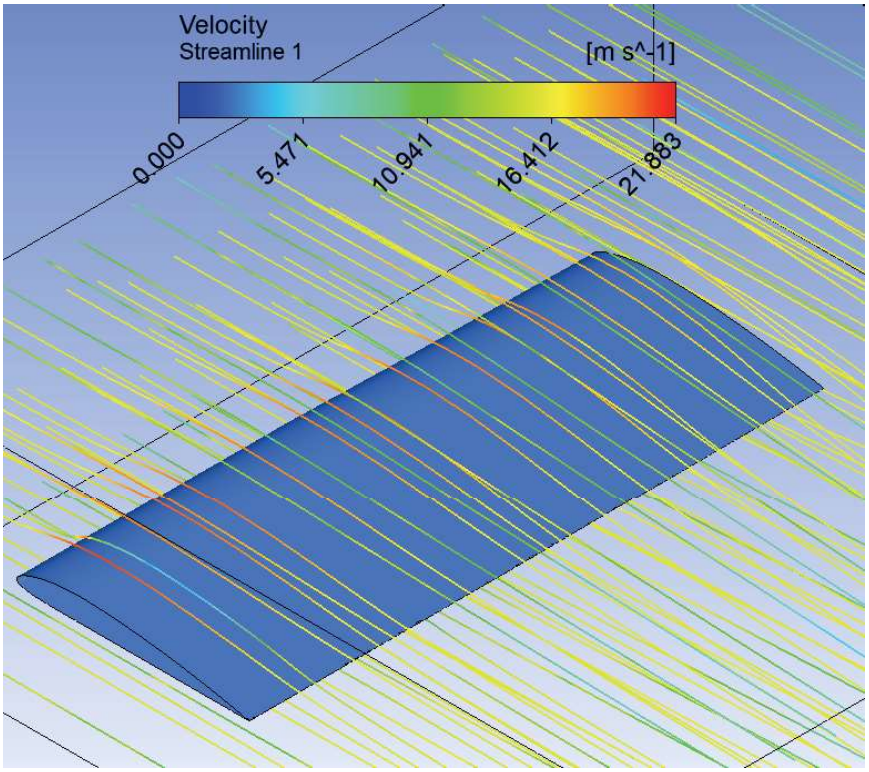

Figure 38: Isometric view of the streamlines over the aerofoil

of the aerofoil and the size of the wing as a whole for the aircraft. The wing simulation also did not contain the planned dihedral present in the final full body design, further emphasizing that the wing simulation is an estimation.

3.2.6 Fuselage

CFD was run on the half fuselage model to show the independent drag force the fuselage is generating, while also ensuring the fuselage wouldnt disrupt the airflow. The results of the drag generated provides an approximate estimation of the thrust required for the fuselage to fly at cruise conditions, which when combined with the drag provided by the wings, provide an estimation of total thrust needed. Based off of the wing simulation, a speed of 16 m/s was simulated using a 0 degree angle of attack. The simulation was halted when the results met the convergence criteria A result of −0.07 N of lift and 0.03 N of drag force was generated from the force plots. The model is half of the fuselage so the drag and lift force of the overall model would be twice the amount of the values found.

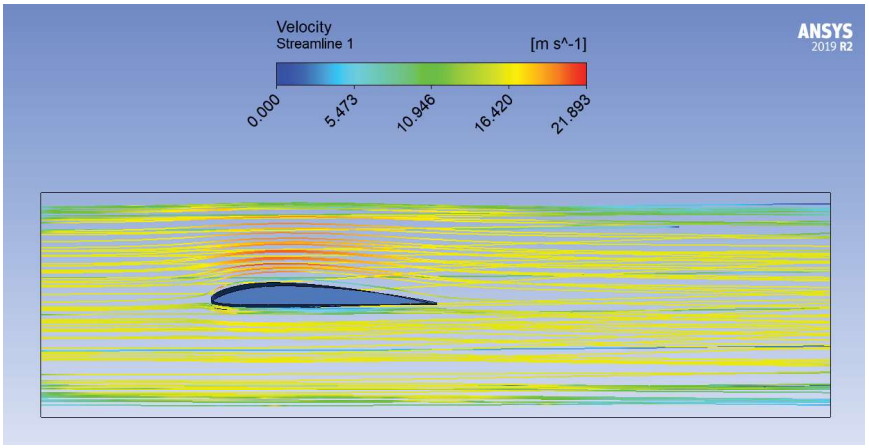

Figure 39: Side-on view of the streamlines over the aerofoil

Therefore, for the overall model, lift force is $-0.14\,\text{N}$ and drag force is $0.06\,\text{N}$. For the calculations it was assumed that the UAV is at the maximum weight of $1.5\,\text{kg}$ and therefore requires $15\,\text{N}$ of lift. A reduction of $0.14\,\text{N}$ is insignificant within the design as it is less than 1 % of the total lift needed. The drag of $0.06\,\text{N}$ shows that the fuselage produces minimal drag when compared to the $0.375\,\text{N}$ that the wings generate The fuselage was also tested to investigate whether the fuselage would form a wake behind the aircraft. A wake is a turbulent airflow that increases drag force on the aircraft, this would greatly increase the thrust required by the aircraft. Therefore, a wake is undesirable within the design.

Figures 40 and 41 show the velocity streamlines flowing around the fuselage. These figures show theres an increase in the velocity under the fuselage, this leads to a higher dynamic pressure along the bottom of the fuselage. From this higher dynamic pressure, a lower static pressure is created causing a negative lift force. Therefore, the streamlines validate the negative lift force shown in the simulation. Figures 40 and 41 also shows that the steamline has re-combine at the end of the fuselage, which shows the fuselage has no wake after the air has flown around the fuselage. The fuselage was designed to minimise the chance of a wake forming behind it, and the CFD simulation serves to validate this design choice.

The fuselage simulation was used as an estimation for the lift and drag conditions of the part at a 0 degree angle of attack utilising the cruise conditions found when performing a CFD on the fuselage. The results found were ideal and so

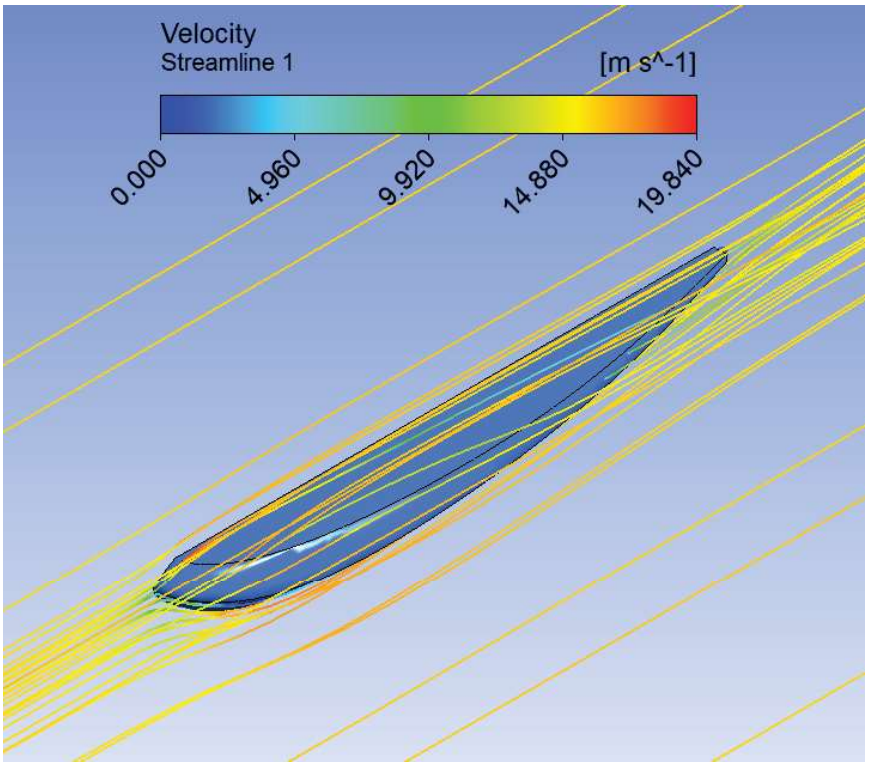

Figure 40: Isometric view of the streamlines over the fuselage

this design for the fuselage was decided to go forward for the final design of the UAV.

3.2.7 Full Body

A CFD simulation was run on the full aircraft for multiple reasons, including determining the flight speed at cruise conditions and ensuring enough there is enough airflow over the control surfaces of the aircraft. In addition, the total drag of the aircraft was needed in order to determine the thrust required. During the full body CFD it was found that the speed needed to generate the required lift was higher than with the wing alone, this could be due to many factors such as the tail providing negative lift, the fuselage blocking some of the effective area of the aerofoil, as well as the fuselage and tail providing negative lift. With the fuselage and aerofoil in place, it was found that a speed of 20 m/s would be needed to generate 15 N of lift when compared to the 16 m/s for the wing alone.

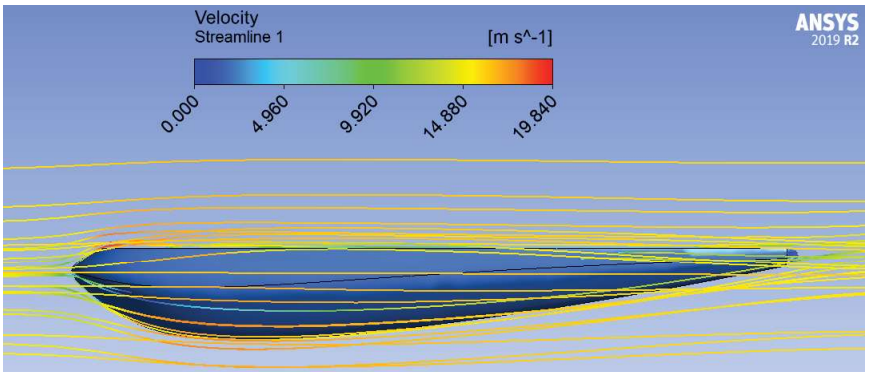

Figure 41: Side-on view of the streamlines over the fuselage

Angle	Lift [N]	Drag [N]
−10	−7.37	1.42
−5	−0.34	0.50
0	6.98	0.50
5	14.40	1.19
10	21.31	2.35
15	26.80	4.16
20	28.04	6.00
25	23.75	8.24

Table 6: Table to show how the lift and drag force varies with the angle of attack

The full body simulation was validated by the previous simulations on the fuselage and aerofoil alone, as the streamlines for these particular parts were similar, this shows the result is repeatable. Once the full body had been validated at 0 degrees angle of attack, the full body could then be run at varying angles of attack from -10 degrees to 25 degrees to investigate the effect of the angle of attack on the lift provided whilst also finding the stall point of the aircraft.

Table 6 shows the value of lift and drag for each respective angle of attack, noting that each value shown is for half a plane and so has to be doubled for the full aircraft.

Figure 43 shows the variation in streamlines as the angle of attack changes. The stall angle was found to be around 20 degrees, as during this streamline it can be seen that a turbulent airflow is forming behind the aerofoil, which

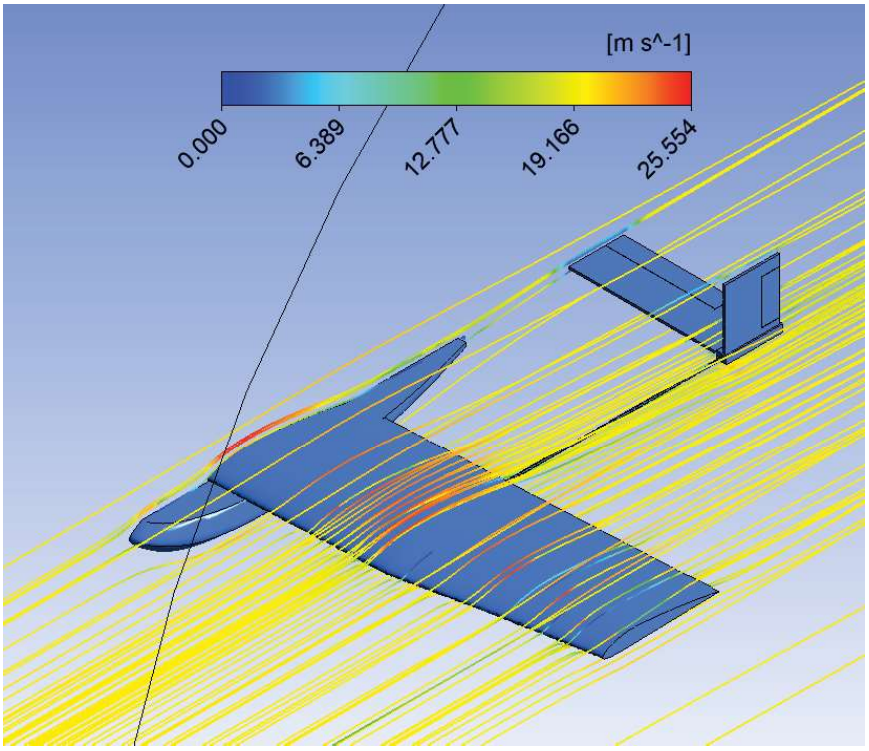

Figure 42: Velocity streamlines over the plane at 0 degrees angle of attack

increases in severity at 25 degrees. This turbulent flow is undesirable as it vastly increases drag acting upon the aerofoil, in addition it also reduces the amount of lift the aerofoil provides. To limit the effect of the turbulent airflow formed, the UAV will not be flying at this angle of attack, and instead will climb using angles of about 15 degrees. A 20 degree angle of stall also matches up to Figure 44 which shows that the graph for lift with varying angle of attack levels off around 20 degrees.

3.2.8 Limitations

Due to limitations within the student version of Ansys available, the mesh isnt as fine as would be desirable due to the 512 000 element limit, and so the simulation run isnt as accurate as would be liked. Therefore, all the values calculated using CFD were taken as an estimation and not as the final value, as the final value can only be obtained by physically testing the part. CFD also doesnt take into account gusts of wind which would most likely be experienced whilst flying

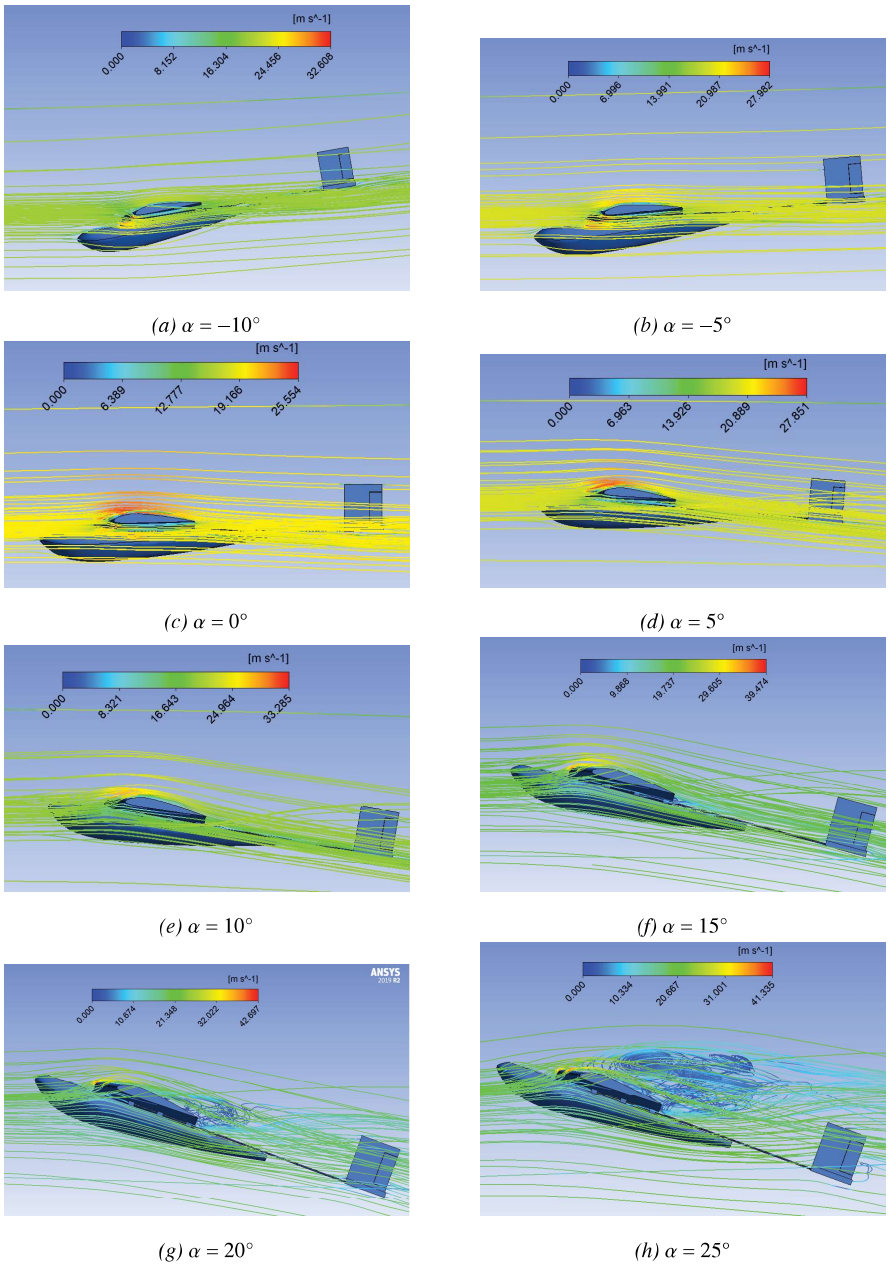

(a) $\alpha = -10°$ *(b)* $\alpha = -5°$

(c) $\alpha = 0°$ *(d)* $\alpha = 5°$

(e) $\alpha = 10°$ *(f)* $\alpha = 15°$

(g) $\alpha = 20°$ *(h)* $\alpha = 25°$

Figure 43: Velocity streamlines at angle of attack, α

which could drastically change the flight characteristics of the UAV.

3.2.9 Flight Simulation

A flight simulator was also run on a Merlin flight simulator in order to perform some final optimisation and validation to the design. In order to obtain an esti-

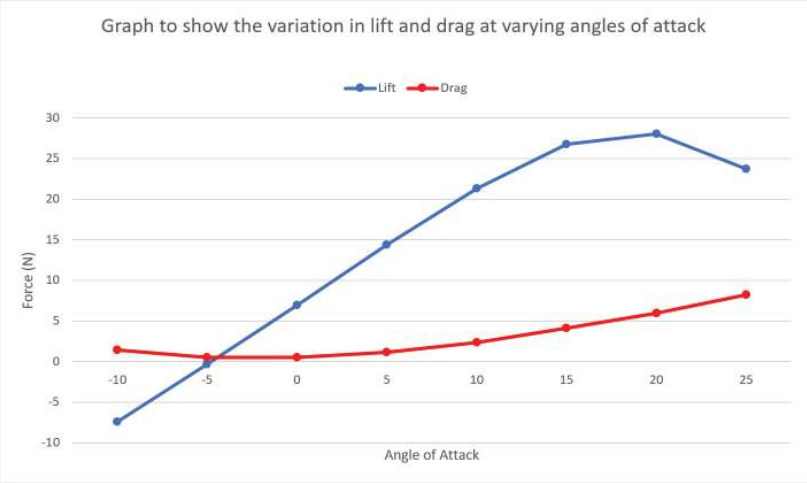

Figure 44: Graph showing the variation in lift and drag at varying angles of attack

mation of the flight characteristics for the design the x and y lengths and mass had to first be scaled up 10 and 100 times respectively, this is due to the fact that the Merlin flight simulator cannot handle low Reynolds numbers very well. Once the UAV had been imported into the Merlin flight simulators, multiple simulations were run slightly editing parameters such as centre of gravity between each simulation, this helped to give an idea of the best position for the centre of gravity for the aircraft. Optimisation was also performed on the size of the control surfaces to ensure they provided enough force to move the aircraft in their respective directions. The flight simulation also served to validate and verify the simulations previously run in CFD, as values such as the stall angle were found to be similar to that provided in the CFD calculation. Finally, the flight simulator also provided the opportunity to test the UAV in windy conditions and to ensure that the wind wouldnt play too much of an effect on the flight performance.

4 The Propulsion System and Electrical Power

4.1 Motor Thrust Calculation

Calculating the thrust the propulsion system needed to provide, first required the resolving of both horizontal and vertical forces acting upon the UAV at